ASEAN Journal of Chemical Engineering 2022, Vol. 22, No. 2, 258 – 273

Effects of Nucleation and Crystal Growth Rates on Crystal Size Distribution for Seeded Batch Potash Alum Crystallization Process

Siti Zubaidah Adnan
Noor Asma Fazli Abdul Samad*
Faculty of Chemical & Process Engineering Technology, Universiti Malaysia Pahang, Lebuhraya Tun Razak, 26300 Kuantan, Pahang, Malaysia
**e-mail:* asmafazli@ump.edu.my

Submitted 15 April 2022 *Revised* 20 October 2022 *Accepted* 30 October 2022

Abstract. The driving force of the cooling crystallization process is supersaturation, where the supersaturation level during the crystallization process is crucial to grow the crystal sufficiently. Nucleation and crystal growth rates are two concurrent phenomena occurring during crystallization. Both are supersaturation functions that determine the growth of seed crystals and the formation of fine crystals. Trade-offs between nucleation and crystal growth are essential for achieving the large size of seed crystals with the minimum number of fine crystals. Thus, the objective of this study is to analyze the effects of nucleation and crystal growth rates on final product quality, which is crystal size distribution (CSD). Modeling of the crystallization process using a potash alum case study is highlighted and simulated using Matlab software. Then, the effects of nucleation rate, crystal growth rate, and both nucleation and crystal growth rates on CSD are evaluated using local sensitivity analysis based on the one-factor-at-a-time (OFAT) method. Based on simulation results for all strategies, a low combined rate delivers the best performance of the final CSD compared to others. Its primary peak has a mean crystal size of 455 μm with 0.0078 m^3/m volume distribution. This means that the grown seed crystals are large with high volume distribution compared to the nominal strategy, which is at the mean crystal size of 415 μm and 0.00434 m^3/m. Meanwhile, the secondary peak has the mean crystal size of 65 μm, 0.00028 m^3/m in volume distribution. This corroborates the least number of fine crystals at the considerably small size compared to nominal's (0.00151 m^3/m, 35 μm). Overall, the low nucleation and crystal growth rates strategy provides useful insights into designing temperature profiles during the linear cooling crystallization process, whereby achievable supersaturation levels in obtaining large crystals with fewer crystal fines are provided via simulation.

Keywords: Crystallization, Crystal Growth Rate, Crystal Size Distribution, Local Sensitivity Analysis, Nucleation Rate, OFAT

INTRODUCTION

Considerable efforts have been established in crystallization as one of the most popular separation and purification operations (Hemalatha et al., 2018, Seki and

DOI: 10.22146/ajche.74121

Su, 2015). Production specifications such as specified size, purity, crystal habit, and crystal size distribution (CSD) of the final crystal product are essential for the crystallization process (Trampuž et al., 2021, Trampuž et al., 2020, Öner et al., 2020). This has led to the establishment of optimization strategies for producing high-quality final products, especially in terms of CSD, to achieve the desired crystal target. CSD has a potent influence on functionality, later processing, and final product properties such as packing (Trampuž et al., 2021, Trampuž *et al*., 2020, Fysikopoulos et al., 2019).

In achieving the desired target, such as uniform CSD, seeding crystallization may offer a better option (Unno and Hirasawa, 2020), particularly for obtaining the large size of crystals (Lee et al., 2019), lessening supersaturation level and suppressing secondary nucleation leading to narrow CSD and high purity of crystals (Penha et al., 2019). Seed addition is required to be implemented within the metastable region in the case of seeded operation to guarantee a growth-dominated process (Nagy et al., 2019). However, even with the reduced supersaturation level achieved by seeding, a high level of supersaturation at the start of the process is inevitable. This is due to the high concentration difference between solute and saturation concentration (Rawlings et al., 1993). This high level of supersaturation causes the high level of nucleation and crystal growth rates, as both rates are supersaturation-dependent. Due to this, along with the grown seed crystals stimulated by the high crystal growth rate, fine crystals are also produced significantly, which is induced by the high nucleation rate. High production of fine crystals may cause the problem in later processing, such as long operational time for filtration and drying of crystals (Öner et al., 2020, Adnan et al., 2019, Seki and Su, 2015), as well as encrustation on internal surfaces of equipment (Acevedo et al., 2019, Lee et al., 2019, Seki and Su, 2015).

In general, nucleation rate can be described as the number of small nanoscopic clusters of crystals formed per unit volume of the solution per second. This process may occur spontaneously or by external forces such as seeding, the interaction between crystals, agitation, and other external forces (Erdemir et al., 2019, Mullin, 2001). Meanwhile, crystal growth rate is the addition of the molecules to the existing crystals at the kink site, which causes changes in size over time (Erdemir et al., 2019, Mullin, 2001). As mentioned earlier, both rates are highly dependable on supersaturation level, which acts as a driving force for these mechanisms to coexist. The high supersaturation level generates more crystal surface area, encouraging faster supersaturation consumption. This consumption contributes to the growth of crystals at large size distribution and increases total crystal mass, forming fine crystals (Rasmuson, 2019). These mechanisms outline the size distribution of crystals. Thus, understanding these individual mechanisms of CSD is significantly valuable in developing the crystallization process.

In addition, to improve understanding of these individual mechanisms in the control of final CSD, the effects of nucleation and crystal growth rates can be studied using local sensitivity analysis. This method allows the impact of input factors' variation to be quantified against model response. The classical approach is by implementing the one-factor-at-a-time (OFAT) method. OFAT enables a less time-consuming approach where useful sensitivity index estimation may still be obtained (Morio, 2011). Many researchers have focused on the impacts of

individual nucleation parameters and crystal growth rates instead of whole mechanisms on final CSD when investigating local or global sensitivity analysis (Wang et al., 2021, Öner et al., 2020, Fysikopoulos et al., 2019, Fysikopoulos et al., 2017).

Meanwhile, implementing OFAT acknowledges individual impacts of nucleation rate on final CSD while the growth rate remains constant and vice versa. This would allow a deeper understanding of the effects of each parameter on final CSD compared to evaluating both parameters as one factor that affects CSD. However, it is known that nucleation and growth rates coexist together; thus, varying both rates concurrently kept the objectivity of this study in line. Trade-offs between these two rates gave a significantly acceptable CSD range for the respective supersaturation control of the crystallization process. This information might offer a new perspective in providing threshold values of the objective function for designing an appropriate supersaturation profile of the cooling crystallization process.

Hence, this paper aims to evaluate the effects of both nucleation and growth rates on the final CSD for seeded batch crystallization process of potash alum. The mathematical model and simulations of the process are developed and conducted in Matlab 2016b software. Potash alum in the water system is adapted from Aamir (2010) as a case study for validation and illustration purposes, and any random system may be chosen. The effects of nucleation and crystal growth rates on final CSD are demonstrated by changing its parameters' value using upper and lower limit values for each respective rate. Local sensitivity analysis using the OFAT method is employed for each rate, then both rates are varied concurrently for further evaluation on the final CSD. The trade-offs between nucleation and crystal growth rates by each strategy for the final CSD of potash alum crystallization are critically discussed in the next section.

THEORY

Mathematical Model

The mathematical model of one-dimensional seeded batch potash alum crystallization process is described briefly in this paper. The main equation for this mathematical modeling is derived from the population balance equation (PBE), as shown in Eq. (1).

$$\frac{\partial n(L,t)}{\partial t} + \frac{\partial n(L,t)G(L,C,T)}{\partial L} = B_{nuc} \qquad (1)$$

This PBE, which is originally in the form of partial differential equations (PDEs), is converted into ordinary differential equations (ODEs) using the method of classes instead of combined quadrature method of moments (QMOM) and method of characteristics (MOCH) as used in Aamir (2010) for simpler computation. The ODEs are shown in Eqs. (2)–(4).

$$\frac{dN_1}{dt} + \frac{G_{x1}}{2\Delta Cl_2}N_2 + \frac{G_{x1} - G_{x0}}{2\Delta \mathrm{C}l_1}N_1 = B_{nuc}, i = 1 \qquad (2)$$

$$\frac{dN_i}{dt} + \frac{G_{xi}}{2\Delta Cl_{i+1}}N_{i+1} + \frac{G_{xi} - G_{xi-1}}{2\Delta Cl_i}N_i + \frac{G_{xi-1}}{2\Delta Cl_{i-1}}N_{i-1} = 0, \quad 1 \le i \le n \qquad (3)$$

$$\frac{dN_n}{dt} + \frac{G_x}{2\Delta Cl}N_n + \frac{G_x}{2\Delta Cl}N_{n-1} = 0, \quad i = n \qquad (4)$$

The kinetic model for secondary nucleation in the power law form from the corrected Becker-Döring relationship, which is adapted from Wölk et al. (2002), is shown in Eq. (5). Meanwhile, the diffusion-controlled size-dependent crystal growth model is shown in Eq. (6). The saturation concentration, C_{sat} equation which is a function of temperature is shown in Eq. (7).

$$B_{nuc} = k_b S^b V \quad (5)$$

$$G_{x_i} = k_g S^g \left(1 + \alpha_g L_{xi}\right)^{\beta_g}, i = 1,2,3\ldots n \quad (6)$$

$$C_{sat} = 3.63 + 0.0243T + 0.00358T^2 \quad (7)$$

$S=(C-C_{sat})/ C_{sat}$ is used for the relative supersaturation, S. Besides, the preliminary seed distribution for this seeded operation that is based on seed sieve size, L_s, is adapted from Aamir (2010), as shown in Figure 1. The initial seed distribution is set at the mean crystal size of 90 µm for demonstration purposes only; thus, any seed distribution is suitable.

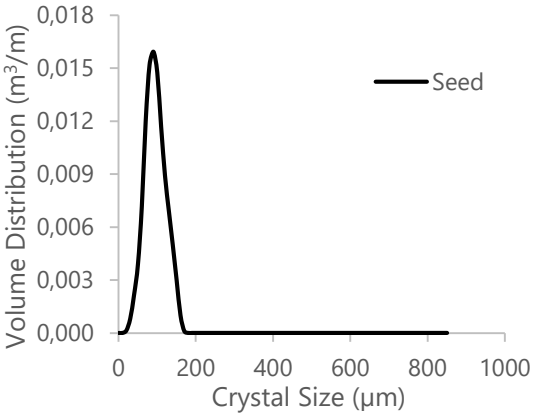

Fig. 1: Initial seed CSD

Model Simulation

This mathematical model for the potash alum crystallization process is then constructed into Matlab software. The backward Euler method, known as 'ode15s' solver in Matlab, is used to solve the model equations as shown in Eqs. (2)-(7). The model parameters used in the process simulation are tabulated in Table 1.

Table 1. Value of kinetic parameters for potash alum crystallization process (Aamir, 2010)

Parameters	Nominal Values	Confidence Interval
k_b	0.0380	±0.044
b	3.4174	±0.037
k_g	8.5708	±0.036
g	1.0000	±0.095
α_g	0.0050	±0.0035
β_g	1.5777	±0.079

One-Factor-at-a-Time (OFAT) Method

This method pursues one factor in each set of experiments and is repeated in turn for all the factors considered for optimizing the model response (Frey et al., 2003). Frey et al. (2003) described the OFAT rules as follow:

i. Commence with a baseline set of factor levels and assess the response.
ii. Change the factor to each of its levels that have not yet been tested, keeping other factors constant.

For this study, the OFAT method is used to demonstrate the effects of nucleation and crystal growth rates. For example, to study the effects of high nucleation rate:

i. Upper bound values for nucleation constants k_b, b, and k_g are calculated by adding the confidence interval value with the nominal value from Table 1 for each nucleation constant.
ii. The crystallization process is simulated while crystal growth rate (g, α_g, β_g) remains constant. The result is then analyzed.

The same rules above are applied to study the effects of other factors in this study. The nucleation and crystal growth effects are investigated via open-loop control on the

potash alum crystallization process. These simulations are categorized into several parts:

i. Case Study 1: Vary nucleation rate; fix crystal growth rate
ii. Case Study 2: Vary crystal growth rate; fix nucleation rate
iii. Case Study 3: Vary both nucleation and crystal growth rates

Model Validation

In this section, open-loop simulation of the nominal potash alum crystallization process is simulated for model validation purposes against published literature. The linear cooling policy is used by adapting nominal values, as shown in Table 1. The linear cooling policy is adapted as it has an almost similar trend to the experimental data of Aamir (2010). Thus, Figure 2(a) shows the temperature profile of nominal potash alum crystallization represented by a solid line which is plotted against the temperature profile of Aamir (2010) (dotted line). Both temperature profiles show the process is being cooled down from 40 to 17°C. The nominal temperature profile depicts a linear descending trend of temperature. Meanwhile, the temperature profile of Aamir (2010) shows the almost linear profile but has a slow cooling down of the solution from 36.5 to 34.8°C at 15 to 30 minutes of operation before linearly cooling down to 17°C.

Next, the nominal saturation concentration profile, as shown in Figure 2(b), was dropped gradually from 0.104 to 0.0051 g of solute/g of water which follows the trend of its temperature profile. Potash alum concentration profile was dropped even slower than the saturation concentration profile, following the same drop of concentration from 0.104 to 0.0052 g/g of water. The distance between solute and saturation concentration profiles representing supersaturation level is shown in Figure 2(c).

The supersaturation profile for nominal strategy, as shown in Figure 2(c), has the linear increment at the beginning of the process until 36 minutes of operation. Then, the profile decreases afterward until the end of the process, following the corresponding distance between solute and saturation profiles in Figure 2(b). As supersaturation level controls the nucleation and crystal growth rates (high supersaturation level means high nucleation and crystal growth rates), the resultant final CSD of potash alum crystallization is plotted against the final CSD of Aamir (2010) in Figure 2(d).

Since the temperature profile is a bit different between the nominal strategy and published literature, the final CSD of each profile is expected to be different too. Figure 2(d) shows that the seed crystals of the nominal case strategy have grown from the mean crystal size of 90 to 415 μm, which is almost similar to Aamir (2010) at the mean crystal size of 410 μm. This growth of seed crystals is contributed by the high crystal growth rate caused by the high supersaturation level, as shown in Figure 2(c). In addition, the secondary peaks that exist at the mean crystal size lower than 200 μm resulted from the high nucleation rate during the high supersaturation level. This indicates that the nominal strategy produced a smaller size of fine crystals, which is at mean crystal size of 35 μm compared to Aamir (2010) at the mean crystal size of 130 μm. In summary, it can be said that the nominal model developed for this work is comparable to Aamir (2010). Thus, the model simulation of this work is considered validated and can be used for further simulation.

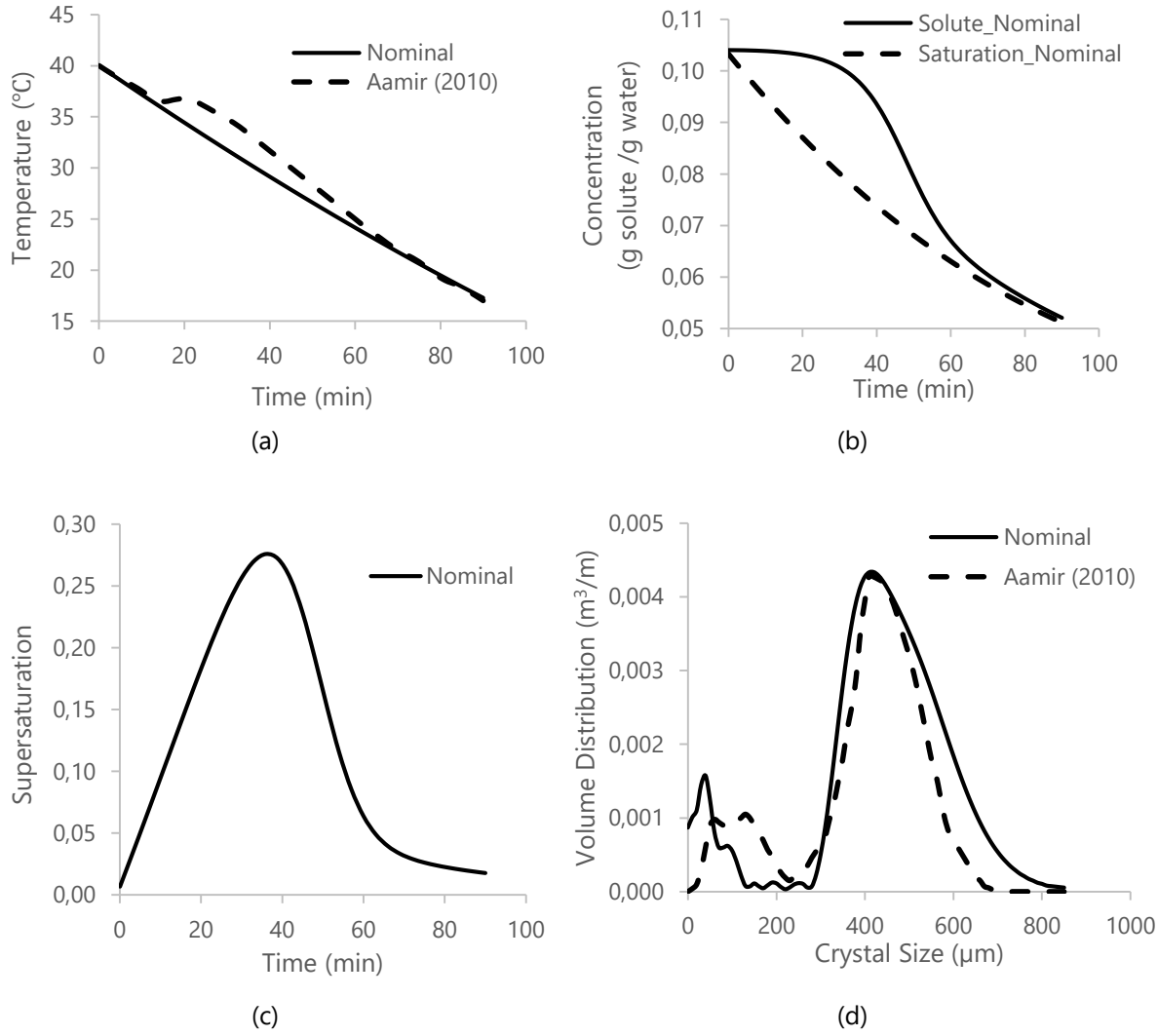

Fig. 2: (a) Temperature profiles of nominal strategy against Aamir (2010), (b) concentration profiles, (c) supersaturation profile, and (d) CSD profile of nominal strategy against Aamir (2010)

RESULTS AND DISCUSSION

Effects of Nucleation Rate

The simulation results of potash alum crystallization for the effects of nucleation rate are shown in Figure 3. The results are obtained by manipulating the nucleation rate using upper and lower bound values of nucleation constant in Table 1, while the crystal growth rate remains constant. As shown in Figure 3(a), temperature profiles of potash alum crystallization portray the descending linear cooling trend for nominal, high, and low nucleation rate strategies. The temperature dropped linearly from 40 to 17°C for all cases, thus can be said that temperature is unaffected by the changes in nucleation rate.

Also, no visible changes in saturation concentration are observed in Figure 3(b), but there is a slight change in potash alum concentration for profiles of high and low nucleation rates. However, all were dropped accordingly from 0.104 to 0.052 g of solute/g of water.

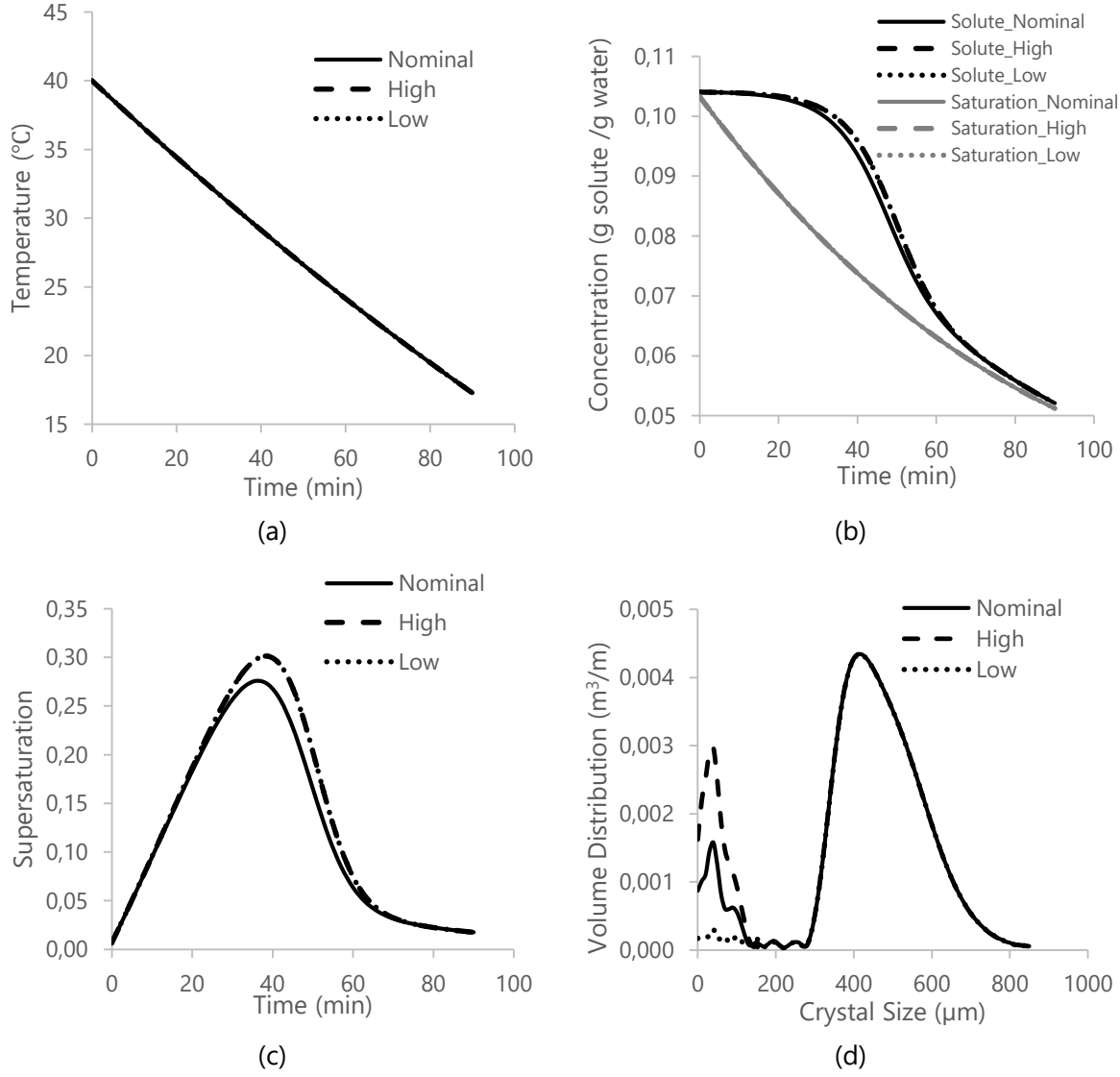

Fig. 3: (a) Temperature, (b) concentration, (c) supersaturation, and (d) CSD profiles for the effects of nucleation rate

Meanwhile, the fact that concentration is temperature dependent is further verified by the saturation concentration profiles (grey lines) that follow the decreasing trend of the temperature profile.

Other than that, supersaturation profiles, as shown in Figure 3(c) for the case of changes in nucleation rate, show the corresponding profile of the distances between solute and saturation concentrations in Figure 3(b). The peak of supersaturation for high and low nucleation is at 39 minutes with the value of 0.301, exactly when the solute concentration starts to descend rapidly. The peak of the nominal supersaturation profile is at 36 minutes of operation with a value of 0.276. The slight difference between each change versus the nominal profile demonstrates solid proof for nucleation as a supersaturation dependent kinetic.

It is noted that the final CSD in Figure 3(d) has different secondary peaks for all cases, which range from mean crystal size 0 to

160 µm, but with similar primary peaks. The volume distribution of the secondary peak for the high nucleation rate is at 0.00294 m^3/m, while for the low nucleation rate is at 0.00030 m^3/m, and the nominal is at 0.00151 m^3/m. Changes in nucleation rate mean there are changes in supersaturation level, contributing to increment or decrement of fine crystals' amount. These results are in agreement with the theory by Erdemir et al. (2019), where supersaturation influences the nucleation rate.

Effects of Crystal Growth Rate

Figure 4 displays the simulation results of manipulating the crystal growth rate for the potash alum crystallization process while the nucleation rate is kept constant. Figure 4(a) demonstrates the temperature profile of nominal, high, and low crystal growth rate cases where the solution's temperature slowly decreases from 40 to 17°C. Temperature profiles for high and low crystal growth rates reported similar trends with the nominal case.

However, concentration trends in Figure 4(b) testified differently, where the apparent differences are the trends for the solute concentration of all cases. Meanwhile, the saturation concentrations remain unchanged. For the case of high crystal growth rate, the solute concentration starts to drop rapidly at time 30 minutes and dropped from 0.104 to 0.052 g of solute/g of water. Meanwhile, for the low crystal growth rate, the rapid decrement of solute concentration starts at 54 minutes of operation, and the solute concentration was decreased from 0.104 to 0.057 g of solute/ g of water.

The resulting supersaturation profiles, as shown in Figure 4(c) (tallied by the distances of solute and saturation concentration in Figure 4(b)), describe the impact of crystal growth rate on the supersaturation level. Indirectly, this indicates that crystal growth rate is also the supersaturation dependent kinetic. The lowest peak of supersaturation is for the case of the high crystal growth rate. This may be because the crystal growth rate dominates the whole crystallization process, thus limiting the nucleation rate (Rasmuson, 2019). It is demonstrated in Figure 4(d), where small size of crystals and the low number of fine crystals were obtained.

Seed crystals, for the case of high crystal growth rate, have been grown from the mean crystal size of 90 to 370 µm, with an additional 10 µm secondary peak. The volume distribution is 0.0035 m^3/m for the primary and 0.0009 m^3/m for the secondary peak. For the case of low crystal growth rate, the seed crystals have been grown from the mean crystal size of 90 to 455 µm. An additional secondary peak of 50 µm was formed by secondary nucleation due to the interaction between crystals that may break into smaller crystal sizes (Erdemir et al., 2019). The volume distribution for its primary peak is 0.00786 m^3/m and the secondary peak is 0.00396 m^3/m, respectively. Overall, the final CSD from nominal value is better compared to the final CSD of others. High crystal growth case has smaller crystals at both primary and secondary peaks.

Meanwhile, low crystal growth case has enormous number of fine crystals even with large size of grown seed crystals. This may because of its supersaturation level that is too high which encourages more formation of fine crystals. Lowering crystal growth rate may cause increment in nucleation rate which causes the increased in concentration, thus increasing supersaturation level (Erdemir et al., 2019). This is also known as supersaturation consumption (Rasmuson,

2019).

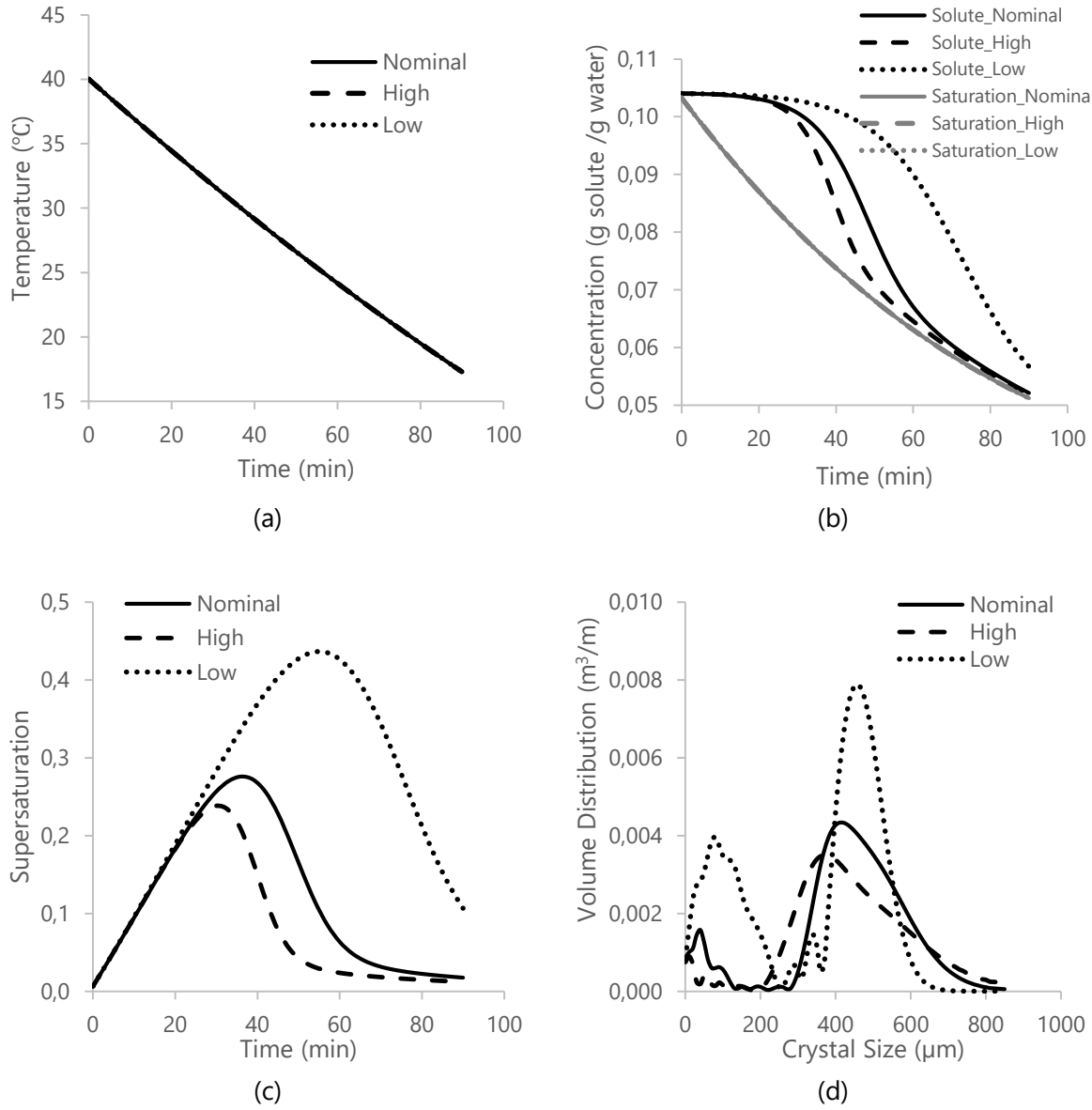

Fig. 4: (a) Temperature, (b) concentration, (c) supersaturation, and (d) CSD profiles for the effects of crystal growth rate

Effects of Nucleation and Crystal Growth Rates

Simulation results for the effects of nucleation and crystal growth rates are shown in Figures 5 to 6. Temperature profiles for all cases, as shown in Figure 5(a), are similar to each other. This is consistent with the results in the previous sub-section that temperature is unaffected by both changes in nucleation and crystal growth rates. Also, it proves that nucleation and crystal growth rates are not temperature dependent, unlike other factors such as concentration and supersaturation. Thus, the solution temperature for all the cases decreased linearly from 40 to 17°C.

Nevertheless, concentration profiles for the high and low combined rates for the potash alum crystallization process are shown in Figure 5(b). In the case of both rates being high, it is observed that its solute concentration has a similar trend with the

high crystal growth rate strategy in Figure 4(b). It starts to decrease rapidly at 30 minutes of operation until it becomes saturated shortly after. Solute concentration was descended accordingly from 0.104 to 0.052 g of solute/ g of water. In the case of both rates being low, the solute concentration has a similar trend with the low crystal growth rate strategy, as shown in Figure 4(b). It decreases gradually at the beginning from 0.104 to 0.095 g of solute/ g of water until an operational time of 54 minutes. Then, it rapidly descends to 0.057 g of solute/g of water until the end of the process. Besides, since saturation concentration is temperature dependent, both saturation profiles have similar trends with their respective temperature profile.

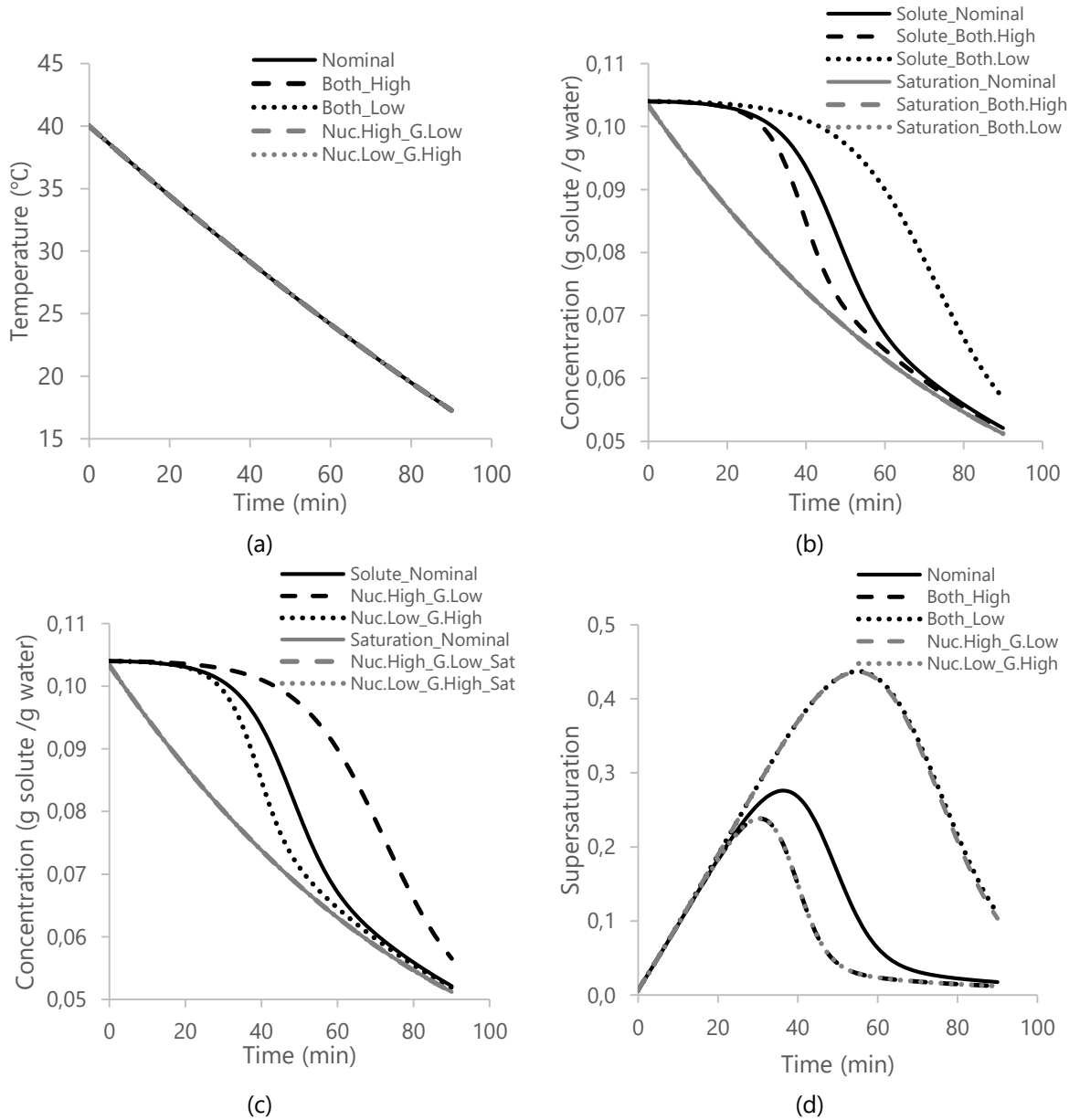

Fig. 5: (a) Temperature profiles, (b) concentration profiles for both high and both low rates, (c) concentration profiles for high nucleation and low crystal growth rate, and vice versa, and (d) supersaturation profiles for the effects of nucleation and growth rates

Consequently, Figure 5(c) demonstrates concentration profiles for the effects of nucleation and growth rates against nominal concentration profiles. It is observed that the solute concentration profile for the case of high nucleation with the low crystal growth rate has a similar trend with low combined rates. Also, the potash alum concentration profile of low nucleation with the high crystal growth rate has a similar trend with high combined rates. It seems that crystal growth rate has major control on the trend of solute concentration compared to nucleation rate. This is indirectly linked to the simulation result of the discrete effect of nucleation rate in Figure 3(b), in which only slight changes in the solute concentration are observed since it has been mentioned earlier that saturation concentration is temperature dependent, no observable changes on saturation concentration caused by the changes in nucleation and growth rates.

Nonetheless, supersaturation profiles shown in Figure 5(d) are the resultant data of the concentration data in Figures 5(b) and 5(c). Since the high combined rates and low nucleation with high crystal growth rate strategies have similar concentration data, their respective supersaturation trends in Figure 5(d) are also similar. The supersaturation peak is at 30 minutes of the operation with the value of 0.238. Also, since both rates are low and high nucleation with low crystal growth rate shares similar trends of concentration data, its respective supersaturation profile is thus similar. The peak is 54 minutes of operation with a supersaturation value of 0.436.

As the final CSD profile is directly associated with the level of supersaturation, Figure 6 exhibits the consequent CSD profiles for the effects of nucleation and growth rates. Figure 6(a) demonstrates the final CSD of high and low combined rates cases. It is noted that the seed crystals of mean crystal size 90 μm have been grown to the ranges of 200 to 850 μm with undesirable fine crystals of mean crystal size below 200 μm. For the case of high combined rates, the primary peak is at the mean crystal size of 365 μm and volume distribution of 0.00350 m^3/m. Meanwhile, the mean crystal size and volume distribution of the secondary peak are at 5 μm and 0.00160 m^3/m. For the case of the low-combined rates, the primary peak has the mean crystal size of 455 μm and the volume distribution of 0.00786 m^3/m. Meanwhile, the secondary peak has the mean crystal size of 65 μm and the volume distribution of 0.00028 m^3/m.

Figure 6(b) displays the final CSD of high nucleation with low crystal growth rate and low nucleation with high crystal growth rate cases. For the case of high nucleation with the low crystal growth rate, it is noted that the seed crystals have grown from the mean crystal size of 90 to 455 μm with the volume distribution of 0.00789 m^3/m. This is represented by the primary peak ranging from 200 to 850 μm. However, the second peak ranges from 0 to 200 μm with the significant volume distribution of 0.00804 m^3/m. This secondary peak has a higher volume than the primary peak. For low nucleation with the high crystal growth rate strategy, the seed crystals were grown to the mean crystal size of 375 μm and volume distribution of 0.00350 m^3/m. The secondary peak has the mean crystal size of 55 μm and the volume distribution of 0.00026 m^3/m.

Overall, low combined rates are the best performance among all cases in this sub-section. It has unified large-grown seed crystals and the insignificant number of fine crystals. Meanwhile, the worst performance case is high nucleation with the low crystal

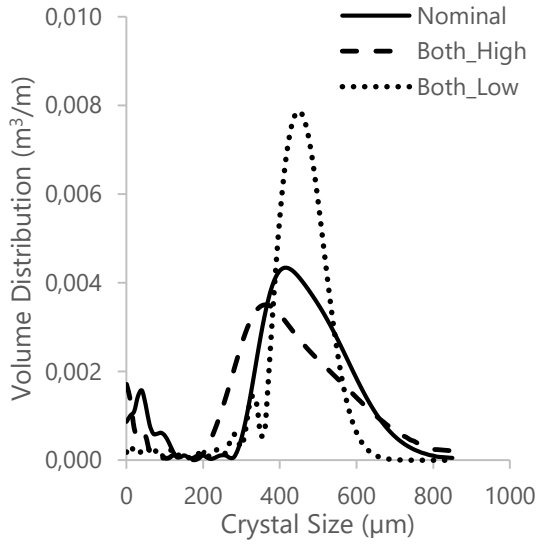

(a)

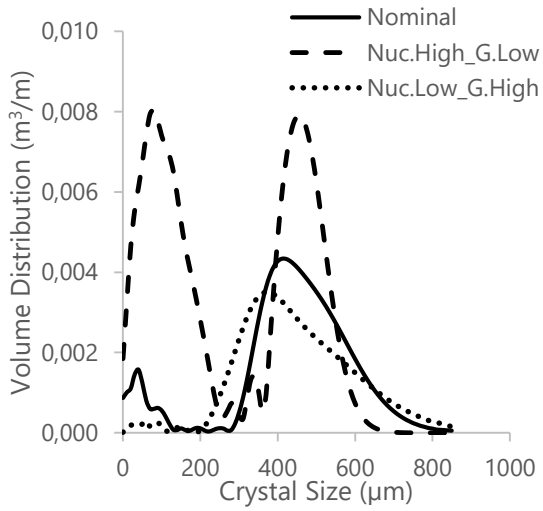

(b)

Fig. 6: (a) CSD profiles for the effects of high and low combined rates, and (b) for the effect of high nucleation and low crystal growth rate, and vice versa

growth rate, where it has a massive number of fine crystals despite having unified large-grown seed crystals. Unified distribution is good, but significant amounts of fine crystals are not favorable for crystallization. It will slow down the filtration and drying process, cause encrustation in the heat exchanger and other issues (Trampuž et al., 2020, Öner et al., 2020, Adnan et al., 2019, Fysikopoulos et al., 2019, Seki and Su, 2015). These results presented an insight into developing a unified final CSD with minimum amounts of fine crystals by lowering both nucleation and crystal growth rates.

Performance Evaluation

Table 3 summarizes the performance of all strategies used in this work. It can be observed that the best performance compared to all strategies in terms of both primary and secondary peaks is still the case of the low combined rates strategy.

The mean crystal size is 455 μm for the primary and 65 μm for the secondary peak, and volume distribution of 0.00786 m^3/m and 0.00028 m^3/m, respectively.

Therefore, it can be concluded that to obtain large unified crystals with the least amounts of fine crystals, nucleation and crystal growth rate are required to be set as low as possible. However, directly setting and controlling both rates is impossible in the case of industrial crystallizers, even for laboratory experimentation. Nucleation and crystal growth rates can only be controlled by manipulating concentration (supersaturation level), which is usually done by controlling temperature. The manipulation of temperature to obtain low combined rates is quite hard. There is no linear manipulation, even from the model equation of nucleation and crystal growth kinetics. In addition, lowering supersaturation to lower both rates may induce supersaturation by consumption, which is mentioned in the previous sub-section. The low crystal growth rate will cause the nucleation rate to increase. This will trigger solute concentration to increase and multiply the supersaturation level (Erdemir et al., 2019, Rasmuson, 2019). Selecting the second-best strategy, which is the constant of this study, or implementing a cubic

Table 3. Comparison of volume distribution and mean crystal size for all strategies for the effects on nucleation and crystal growth rates

	Volume Distribution (m^3/m)		**Mean Crystal Size (μm)**	
	Primary	Secondary	Primary	Secondary
Constant	0.00434	0.00151	415	35
High Nucleation	0.00434	0.00294	415	35
Low Nucleation	0.00434	0.00030	415	40
High Crystal Growth	0.00350	0.00090	370	10
Low Crystal Growth	0.00786	0.00396	455	80
High Nucleation & High Crystal Growth	0.00350	0.00160	365	5
Low Nucleation & Low Crystal Growth	0.00786	0.00028	455	65
High Nucleation & Low Crystal Growth	0.00789	0.00804	455	80
Low Nucleation & High Crystal Growth	0.00350	0.00026	375	55

cooling policy suggested by Lee et al. (2019) to regulate the supersaturation level might be a better choice.

Nevertheless, based on the results in this paper, threshold values for the objective function that corresponds to the temperature trajectory may be developed for obtaining large CSD with minimum fines. Also, even though the potash alum crystallization process is used in this paper, implementing these results on other crystallization systems is encouraged. This is because the crystallization process inevitably involves both mechanisms at the molecular level.

Thus, it can be said that by performing local sensitivity analysis on nucleation and crystal growth rate, a proper temperature trajectory may be established for the seeded batch cooling crystallization system.

CONCLUSIONS

The effects of nucleation and crystal growth rates on final crystal size distribution (CSD) for seeded batch potash alum crystallization are thoroughly analyzed in this paper. The simulations performed in Matlab software involve three parts: the effects on nucleation rate, crystal growth rate and both rates simultaneously using the one-factor-at-time (OFAT) method. From simulation results, low combined rates provided the best profile with unified (high volume distribution at 0. 00786 m^3/m) and large CSD (455 μm) with the least number of fine crystals (0.00028 m^3/m, 65 μm). The nominal CSD presented the best achievable profile among other strategies. It has large-grown seed crystals at the mean crystal size of 415 μm (0.00434 m^3/m) and the minimum number of fine crystals at 35 μm with 0.00151 m^3/m volume distribution. However, other strategies, such as high nucleation with low crystal growth rate, provide better performance of primary CSD with the mean crystal size of 455 μm and volume

distribution of 0.00789 m^3/m but not in terms of the secondary peak. Low nucleation with the high crystal growth rate strategy delivered a better performance of the secondary peak (but not the primary peak) at the volume distribution of 0.00026 m^3/m. These trade-offs between nucleation and crystal growth rates provide valuable insight into designing temperature trajectories where moderately low nucleation and crystal growth rates could be obtained. Thus, future research should consider designing achievable temperature trajectories that could provide large-grown seed crystals with minimum fine crystals.

ACKNOWLEDGEMENT

The financial support provided by Universiti Malaysia Pahang (UMP) under Doctorate Research Scheme (DRS) is duly appreciated.

NOMENCLATURE

B_{nuc}	:	rate of nucleation [number of particles cm^{-3} min^{-1}]
b	:	order of nucleation
C	:	concentration of solute [g of solute g solvent $^{-1}$]
C_{sat}	:	concentration at saturation condition [g of solute g solvent $^{-1}$]
G	:	rate of crystal growth [μm s^{-1}]
G_x	:	rate of crystal growth rate in length direction [μm s^{-1}]
g	:	order of crystal growth
k_b	:	kinetic coefficient for nucleation [number of particles cm^{-3} min^{-1}]
k_g	:	kinetic coefficient for crystal growth [number of particles cm^{-3} min^{-1}]
L	:	length of crystal particles [μm]
L_s	:	sieve size [μm]
L_x	:	length of crystal particles in the direction of *x* [μm]
n	:	relative shape function of crystals
N_i	:	number of crystals for class i per suspension unit [number of particles cm^{-3}]
S	:	supersaturation
S^b	:	supersaturation for nucleation
S^g	:	supersaturation for crystal growth
T	:	temperature of the solution in the crystallizer [℃]
t	:	time of crystallization [min]
V		mean volume of crystal [cm^3]
α_g	:	parameter for crystal growth
β_g	:	parameter for crystal growth
ΔCl_i	:	size of class for *i*th classes [μm]

REFERENCES

Aamir, E., 2010. Population Balance Model-Based Optimal Control of Batch Crystallisation Processes for Systematic Crystal Size Distribution Design. *PhD thesis*. Loughborough University, Leicestershire, England

Acevedo, D., Yang, X., Liu, Y.C., O'Connor, T.F., Koswara, A., Nagy, Z.K., Madurawe, R., and Cruz, C.N., 2019. "Encrustation in continuous pharmaceutical crystallization processes - a review." *Org. Process Res. Dev.*, *23*, 1134–1142.

Adnan, S.Z., Saleh, S., and Samad, N.A.F.A., 2019. "Evaluation of controlled cooling for seeded batch crystallization incorporating dissolution," in: *AIP Conference Proceedings*. AIP Publishing, pp. 020042–1–020042–8.

Erdemir, D., Lee, A.Y., and Myerson, A.S., 2019. "Crystal Nucleation," in: Handbook of Industrial Crystallization. Cambridge

University Press, pp. 76–114.

Frey, D.D., Engelhardt, F., and Greitzer, E.M., 2003. "A role for 'one-factor-at-a-time' experimentation in parameter design." *Res. Eng. Des.*, 14, 65–74.

Fysikopoulos, D., Benyahia, B., Borsos, A., Nagy, Z.K., and Rielly, C.D., 2019. "A framework for model reliability and estimability analysis of crystallization processes with multi-impurity multi-dimensional population balance models." *Comput. Chem. Eng. 122*, 275–292.

Fysikopoulos, D., Borsos, A., Li, W., Onyemelukwe, I., Benyahia, B., Nagy, Z.K., and Rielly, C.D., 2017. "Local vs global estimability analysis of population balance models for crystallization processes." *Comput. Aided Chem. Eng., 40*, 55–60.

Hemalatha, K., Nagveni, P., Kumar, P.N., and Rani, K.Y., 2018. "Multiobjective optimization and experimental validation for batch cooling crystallization of citric acid anhydrate." *Comput. Chem. Eng., 112*, 292–303.

Lee, A.Y., Erdemir, D., and Myerson, A.S., 2019. "Crystals and Crystal Growth," in: Handbook of Industrial Crystallization. Cambridge University Press, pp. 32–75.

Morio, J., 2011. "Global and local sensitivity analysis methods for a physical system." *Eur. J. Phys., 32*, 1577–1583.

Mullin, J.W., 2001a. "Nucleation," in: Crystallization. Elsevier, pp. 181–215.

Mullin, J.W., 2001b. "Crystal growth," in: Crystallization. Elsevier, pp. 216–288.

Nagy, Z.K., Fujiwara, M., and Braatz, R.D., 2019. "Monitoring and Advanced Control of Crystallization Processes," in: Handbook of Industrial Crystallization. pp. 313–345.

Öner, M., Stocks, S.M., and Sin, G., 2020. "Comprehensive sensitivity analysis and process risk assessment of large scale pharmaceutical crystallization processes." *Comput. Chem. Eng., 135*, 106746.

Penha, F.M., Zago, G.P., and Seckler, M.M., 2019. "Strategies to control product characteristics in simultaneous crystallization of NaCl and KCl from aqueous solution: Seeding with KCl." *Cryst. Growth Des.. 19*, 1257–1267.

Rasmuson, Å.C., 2019. "Crystallization Process Analysis by Population Balance Modeling," in: Handbook of Industrial Crystallization. pp. 172–196.

Rawlings, J.B., Miller, S.M., and Witkowski, W.R., 1993. "Model Identification and control of solution crystallization processes - a Review." *Ind. Eng. Chem. Res., 32*, 1275–1296.

Seki, H., and Su, Y., 2015. "Robust optimal temperature swing operations for size control of seeded batch cooling crystallization." *Chem. Eng. Sci. 133*, 16–23.

Trampuž, M., Teslić, D., and Likozar, B., 2021. "Crystal-size distribution-based dynamic process modelling, optimization, and scaling for seeded batch cooling crystallization of Active Pharmaceutical Ingredients (API)." *Chem. Eng. Res. Des., 165*, 254–269.

Trampuž, M., Teslić, D., and Likozar, B., 2020. "Process analytical technology-based (PAT) model simulations of a combined cooling, seeded and antisolvent crystallization of an active pharmaceutical ingredient (API)." *Powder Technol., 366*, 873–890.

Unno, J., and Hirasawa, I., 2020. "Partial seeding policy for controlling the crystal quality in batch cooling crystallization." *Chem. Eng. Technol., 43*, 1065–1071.

Wang, L.G., Morrissey, J.P., Barrasso, D., Slade, D., Clifford, S., Reynolds, G., Ooi, J.Y., and Litster, J.D., 2021. "Model driven design

for twin screw granulation using mechanistic-based population balance model." *Int. J. Pharm., 607*, 120939.

Wölk, J., Strey, R., Heath, C.H., and Wyslouzil, B.E., 2002. "Empirical function for homogeneous water nucleation rates." *J. Chem. Phys., 117*, 4954–4960